Growth of silver on ZnO and SnO_2 thin films intended for low emissivity applications

Rafael Alvarez[a], Juan C. González[a], Juan P. Espinós[a], Agustin R. González-Elipe[a], Ana Cueva[b], Francisco Villuendas[b]

[a]Group of Nanotechnology of Surfaces. Instituto de Ciencia de Materiales de Sevilla (CSIC-USE). Avda. Américo Vespucio 49. 41092 Sevilla (Spain)

[b]Group of Photonic Technologies. Departamento de Física Aplicada, Universidad de Zaragoza, c/ Pedro Cebuna 12, 50009, Zaragoza (Spain)

Corresponding author:

Rafael Alvarez
Tlf.: +34 954 48 95 76
Fax: +34 954 46 06 65
rafael.alvarez@icmse.csic.es

Abstract

In the present work we have investigated the relationships existing between the optical properties and the growth mechanism, microstructure and surface roughness of SnO_2 and ZnO oxide films prepared by magnetron sputtering under conditions resembling those utilized in industry. Thin films of these oxides with different thicknesses were characterized by atomic force microscopy, glancing incidence X-ray diffraction (GIXRD), X-ray reflectometry and spectroscopic Ellipsometry. The roughness evolution of the film properties (density, surface roughness and refraction index) as a function of their thickness has been evaluated within the concepts of the Dynamic Scaling Theory of thin film growth. Zinc oxide films were rougher than tin oxide films of similar

thickness, indicating a different growing mechanism for the two materials. Silver was evaporated onto the surface of the two oxide thin films and its earlier stages of nucleation studied by background analysis of the X-ray photoemission spectra. A different nucleation mechanism was found depending on the nature of the oxide acting as substrate. The superior performance of the zinc oxide based low emissive coatings is related with a better wetting of silver on the surface of this oxide despite the comparatively lower roughness of the tin oxide layers.

Keywords: ZnO and SnO_2 thin films, silver nucleation and wetting, low emissivity coatings, roughness evolution, growth mechanism.

1. Introduction

Low emissivity glasses (low-e glass), used in homes, offices, automobiles, and other applications incorporate an oxide-metal-oxide composite coating that provides a high IR reflectivity.[1] To achieve this functionality, these glasses incorporate a stacked structure consisting typically of a thin metal sandwiched between two oxides thin films. [2,3] This type of structures has been modeled and fabricated for several decades and nowadays represent a commercial product manufactured and sold by different companies all over the world.[4]

Low-e glasses must depict two main features: a high optical transparency in the visible region and a high reflectance in the near-infrared region. Although different metal/dielectric stacking structures have been proposed to achieve this goal, the most common coating structure consists of a silver layer sandwiched

between two transparent oxide layers, usually SnO_2 and ZnO (i.e., MOx/Ag/barrier/MOx structures, where a barrier layer is introduced to avoid the oxidation of the silver layer during the second deposition process of the oxide).[4-6] Important characteristics of glasses incorporating these coatings are a low surface resistivity, a high optical transmittance in the visible and a high energy gap of about 3.6 eV and 3.3 eV, depending on the oxide.

Despite the numerous theoretical modelling[7.8] and experimental investigations[9] dealing with these structures, there is a clear lack of fundamental knowledge relating their performance with critical microstructural characteristics of the system (e.g., roughness of the oxide layers, homogeneity of the metal film, etc.). Thus, only recently there have been some studies addressing systematically the relationship existing between these topographic properties of the individual layers, fundamentally the roughness of the oxide layers, and the final performance of the complete structure.[10] In this regard, flat oxide surfaces seem to improve the transparency of the whole structure and avoid the prevalence of anomalous transmission losses caused by scattering of the light at the metal-oxide interfaces. It is also believed that flat oxide surfaces might contribute to decrease the agglomeration degree of the silver layers and, consequently, reduce its electrical resistance and the emissivity of the whole structure.[11]

Magnetron-sputtering (MS) is likely the most common technique for the large-scale processing of low-e coatings.[12] In principle, one of its recognized advantages is that the ion bombardment effects associated with this technique contribute to smooth the surface of the oxide films and hence to improve the quality of the silver overlayers. However, despite the application of similar

multilayer architectures, it is generally found that ZnO/Ag/barrier/ZnO systems are superior to equivalent SnO_2/Ag/barrier/SnO_2 multilayers in providing an enhanced emissivity and higher transmission in the visible.[13] Trying to unravel the causes contributing to this different behavior, in the present paper we carry out first a systematic study of the evolution with thickness (from 20nm to 800nm) of the roughness and other properties such as density and refraction index of ZnO and SnO_2 thin films prepared by MS on silicon and glass. To approach as much as possible the industrial conditions of preparation of these thin film oxides, deposition conditions have been selected by following the industrial criterion of maximizing the power density of the magnetrons for each oxide. Under these conditions, the growth mechanisms of the two oxides have been critically analyzed by using the concepts of the Dynamic Scaling Theory (DST) of surface growth.[14,15] Then, we have studied the growth processes and wetting efficiency of silver deposited by evaporation on thin film surfaces of these two thin film oxides prepared by MS. For the first part of our study we have used X-ray reflectometry (XRF), X-ray diffraction (XRD), Scanning electron microscopy (SEM), atomic force microscopy (AFM) and spectroscopic ellipsometry. To assess the efficiency of silver to wet these two substrates we have employed the Tougaard´s principles[16,17] to analyze the backgrounds of the X-ray photoemission spectra for successive evaporations of silver on ZnO and SnO_2 thin film surfaces. This procedure permits to ascertain the growing morphology of a given material on rough substrates and, more specifically, if it forms a continuous overlayer or agglomerates in the form of islands.[18,19] A critical evaluation of all these results in comparison with the actual emissivity values determined in real multilayer structures indicates that a better spreading

of silver on the surface of ZnO is the main cause of the lower emissivity of industrial ZnO based multilayers, even if tin oxide films present a lower roughness.

2. Experimental and Methods

ZnO and SnO_2 thin film preparation and characterization

ZnO and SnO_2 layers have been deposited by reactive magnetron sputtering on silicon and soda lime glass substrates under conditions resembling as much as possible those utilized in industry. The used experimental facility consists of a Leybold L-560 vacuum system equipped with 3 inches diameter magnetrons powered by pulsed DC power supplies. The distance between magnetrons and substrates is 250mm and the operating conditions by the reactive sputtering are summarized in Table 1.

The discharge power was selected as 150W and 300 W for SnO_2 and ZnO respectively, because these values are close to the maxima compatible with the magnetron size. These values yield power densities of 6.5 W/cm^2 for ZnO and 3.3 W/cm^2 for SnO_2, quite similar to those used in industry by the manufacturing processes of low-emissivity coating where the dielectric layers are deposited to the maximum possible power. The O_2 partial pressure values were set as the minimum pressures assuring that the deposition is made in the reactive mode yielding stoichiometric films. The selected values were determined from reactive deposition curves determined for each compound and chamber condition. In

our case the optimum values were $5x10^{-4}$ mbar and $8x10^{-4}$ mbar for SnO_2 and ZnO respectively.

The residual vacuum pressure was $5x10^{-6}$ mbar and layers of the two materials were deposited with thicknesses ranging from 20 to 800nm.

The morphology of the oxide thin films was examined by cross section scanning electron microscopy (SEM) for thin films deposited on silicon and then cleaved. Images were taken in a field emission scanning electron Phillips FEG-SEM microscope.

Atomic force microscopy (AFM) images were taken with a Dulcinea microscope from Nanotec (Madrid, Spain) working in tapping mode and using high frequency cantilevers with silicon tip. The root-mean-square (rms) roughness and the height-height correlation function were computed from 10x10μm scans of films with increasing thickness, in order to obtain the roughness (α) and growth (β) exponents used for the dynamic scaling evaluation of thin film growth mechanisms.

Grazing incidence x-ray diffraction (GIXRD) measurements taken for thin films thinner than 100 nm were carried out in a PANalitycal X'Pert Pro MPD diffractometer by using the Cu-K_α radiation at a fixed glazing incident angle of 0.5º and a 2θ ranging from 10º to 80º, with a step size of 0,05º. The Bragg-Brentano X ray diffraction (XRD) analysis of films thicker than 100 nm was performed in a PANalitycal X'Pert Pro MPD diffractometer provided with X'Cellerator detector and graphite monochromator and using the Cu-K_α radiation, 40 kV, 40 mA, in a 2θ range from 10º to 80º and a step of $\Delta 2\theta$=0,016º.

Specular x-ray reflectivity analysis for films with a thickness d<100 nm was carried out in the PANalitycal X'Pert Pro diffractometer working in reflection mode (ω-2θ scan), using the Cu-K_α radiation and a W/Si crystal as parabolic x-ray mirror. The scan axis was ω-2θ and the scan mode was continuous with a scan range from 0.0º to 5.0º and a step size 0.005º. The X'Pert reflectivity program (PANalitycal B.V.) was used to fit the reflectivity raw data. The intensity reflections for ZnO and SnO_2 thin films were modeled by means of a uniform homogeneous layered media with a sharply defined boundary to account for the Si-substrate.

Spectroscopic Ellipsometry (SE) was carried out in a J.A. Woollam VASE (variable angle spectroscopic ellipsometry) spectroscopic ellipsometer. Values of Ψ and Δ were obtained over the spectral range of 300 to 1400 nm, at 2 nm resolution. As a consistency check of the data, the incidence angle was varied at three angles of incidence: 65º, 70º, and 75º degree. Optical modeling and parameter fitting were done with the WASE32© program (J.A. Woollam Co.,Inc.). To model the ellipsometric spectra for a fixed film thickness (thickness values were obtained by transversal SEM images) non-uniformity in thickness and angular spread of the beam entering the detector were taken into account through fitting parameters. Partial polarization or monochromator bandwidth effects were not found. Quality assessment of the fit data was done by imposing that the mean-squared error (MSE) value was below 5 units for all studied samples. The ellipsometric optical model consisted of three layers deposited onto a silicon substrate that accounted for 1) roughness-, 2) Bruggeman effective medium approximation-, and 3) Cauchy- layers. The rough surface layer was assumed to consist of 50% film material and 50% voids. The

Bruggeman effective medium approximation layer was coupled to the Cauchy layer. The Cauchy dispersion equation was used for the transparent region (λ > 500 nm). No dispersion of refractive index and extinction coefficient was considered for 500 < λ < 1400 nm, while for λ < 500 nm one classic Lorentz oscillator was added to the Urbach absorption of the Cauchy dispersion.

Preparation and characterization of MOx/Ag/barrier/MOx low-E structures

Low-E structures were prepared in the same installation Leybold 560, with 3 inch magnetrons, in which ZnO and SnO_2 have been deposited. Deposition conditions of oxide layers are the same as for individual layers. Titanium was used as barrier layer and the silver low emissivity layer was deposited in 10^{-3} mbar Ar atmosphere.

Reflection and transmission coefficients have been obtained in a homemade spectrophotometer, while emissivity has been obtained in a TIR100-2 (Inglass) emissometer as the reflectivity of radiation emitted at 100ºC, and derived from the sheet resistivity measured with an inductive sheet resistivity meter, Nagy SRM-12.[20]

Emissivity at 100ºC was measured in an emissometer (TIR100-2, Inglass) and derived from sheets resistivity measurements (Sheet Resistivity Meter SRM-12, Nagy.

XPS and QUASES analysis of the growth of silver

To study the wetting behavior of silver on the two oxide surfaces, increasing amounts of metallic silver, from a fraction of a monolayer to several monolayers, have been deposited simultaneously on two clean surfaces of ZnO and SnO_2 films of similar thickness (around 20 and 200 nm) for the two materials. Since the results were quite similar irrespective of the thickness of the oxide thin films we only describe in the text the results obtained for the thinnest ones. The simultaneous evaporation on the two substrates ensures that each set of samples contain the same amount of deposited silver. The metal was deposited, step by step, by thermal evaporation from a home-made resistive source, consisting of three wrapped W wires (0.3 mm diameter) with an Ag wire (0.2 mm diameter) wound around. Evaporation was carried out in the preparation chamber of the X-ray photoemission spectrometer, under ultra-high vacuum ($P<10^{-8}$ mbar), at a deposition rate of ~0.1 nm/min, with the substrates kept at room temperature situated at 30 cm from the evaporation source. After each deposition, the samples were transferred to the analysis chamber of the spectrometer under ultra-high vacuum conditions (base pressure, 10^{-10} mbar). Prior to the first deposition stage, the substrates were surface cleaned in situ by treatment with a plasma of O_2/Ar (5% of O_2) obtained with a microwave downstream plasma source, to remove the adventitious carbon contaminating their surface.

XPS spectra were recorded after each Ag deposition step with a VG ESCALAB 210 spectrometer, with the hemispherical energy electron analyzer working in the pass energy constant mode at a value of 30 eV. Non

monochromatic AlKα radiation ($h\nu$ =1486.6 eV) was used as excitation source. The resolution of the spectrometer, as measured by the FWHM of the Ag3d5/2 peak, was 1.1 eV. Binding energy (BE) calibration of the spectra was done by referencing the recorded peaks to the following main peaks of the substrates: $Zn2p_{3/2}$ at 1022.05 eV and $Sn3d_{5/2}$ at 486.6 eV.

The initial states of growth of silver films evaporated in vacuum on SnO_2 and ZnO thin films were studied by detailed analysis of the peak shape of the X-ray photoemission spectra (XPS), following the Tougaard´s methodology.[16,17] Spectra have been analyzed with the QUASES software[21] under the assumption that silver grows in the form of three dimensional islands on the surface of the oxide films. By coalescence of these islands a continuous silver film would be obtained. This analysis implies the study of the evolution of inelastic backgrounds of photoelectron signals when the coverage and thickness of a deposited film grows on the substrate. In all the cases, the Ag3d signal, including both the elastic components and the inelastic tails on the low-kinetic-energy side of them, (binding energy range 340-450 eV), has been used for the XPS peak shape analysis, with the QUASES software package.[21] An inelastic mean free path of 1.61 nm has been estimated for the Ag3d photoelectrons by the TPP2M formula.[22]

3. Results and discussion

Structure and microstructure of oxide thin films

Figure 1 shows FEG-SEM cross-section images for SnO_2 and ZnO thin films deposited on silicon. Although for a thickness higher than 100 nm the two materials present a nanocolumnar microstructure, significant differences can be observed in the microstructure of the two oxide layers for a thickness smaller than this value. A first observation is that the ZnO nanocolumns have a higher width (approximately 40-50nm) than those of the SnO_2 film (approximately 10-20 nm). In addition, the SnO_2 micrograph shows that nanocolumnar growth only starts in this material after the formation of an initial homogeneous layer of *c.a.* 100nm. This homogeneous layer is not found in the case of ZnO where the nanocolumnar microstructure forms directly on the substrate surface.

Figure 2 displays the GIXRD patterns of a series of thin (d<100nm) ZnO and SnO_2 films deposited on silicon. Similar bands could be observed for the same type of films deposited onto glass substrates, although they were superimposed onto a very broad feature attributed to the amorphous substrate. The diffraction peaks recorded for the two samples correspond to the (002) and (110) and (101) planes of the ZnO and SnO_2 films, respectively. By applying the Scherrer equation to the (002) peak it was possible to determine that the average size of the crystalline domains vary from ca. 3-4 nm to 7-8 nm from the thinnest to the ticker films of these two oxide films. For thicker films (d>400 nm), the diffraction diagrams recorded in a conventional Bragg- Brentano configuration evidenced the development of (102) planes for ZnO and (211), (220) and (002) planes for SnO_2. These relatively wide peaks indicate a small size of the crystalline

domains. These diagrams also sustain the absence of a clear preferential texturing, except for ZnO where some texturing according to the (002) plane could be observed. A summary of the main structural parameters deduced from this analysis is reported in Table 2.

Measured X Ray reflectivity curves corresponding to films with 20nm, 50 nm and 100nm thickness are shown in Figure 3 together with the theoretical curves deduced by fitting. The rapid attenuation of the interference oscillations observed in ZnO can be linked with a more imperfect packing morphology of these oxide thin films, likely very much influenced by the higher power density for their synthesis (see experimental section). Conversely, the slower attenuation in the interference oscillations in the SnO_2 samples can be accounted for by assuming a more homogenous and better packed layer. The different slope of the profiles and the measured critical angles (i.e., 0,06º and 0.10º for ZnO and SnO2 films, respectively) also support this assessment. Hence, to get a good fitting of the experimental curves, the ZnO and SnO_2 films were respectively modeled by means of three- and one-uniform layers with sharply defined boundaries among them and with the Si-substrate in the former case. Simulations were done by adjusting of three parameters for these individual layers: surface and interface roughness, interfaces quality and density variations with thickness. This model allowed us to deduce variations of film density with depth in the case of ZnO (i.e. three layers of varying characteristics) and to determine values of the interface and surface roughness for the two oxides. For the whole set of investigated films the calculated thickness of the ZnO model layers, resulting from the accumulation of individual

layers, was of 17.15 nm, 45.86, and 90.06nm, with overall densities varying negatively by 8, 2 and 6% with respect to the ZnO bulk value of 5.06g/cm^3. In the case of SnO_2 samples, we considered that the density was constant through the whole layer thickness, with a value varying negatively from 15% to 1% with respect to the bulk value of 6.95 g/cm^3 as the film thickness increases from 20nm to 100nm. The obtained parameter values are listed in Table 2. The results outlined before show an effective increase in density with the film thickness. Also, the surface roughness resulted constant for ZnO with a value of around 1nm, but increased from 0.5nm to 1nm for the SnO_2 films. It is worthy of note that under the assumptions adopted for the simulation, the nominal thicknesses of the films could be reproduced reasonably well with values of 17.1 nm, 45.9 nm and 90.1 nm for the ZnO samples and 20.9nm, 51.4nm and 106.7 nm for the SnO_2 samples. Meanwhile, although surface roughness values are in all cases close to the sensitivity of the technique, it seems that in this range of low thickness the surface roughness of the SnO_2 thin films increases with the thickness of the films, while ZnO films present rather constant roughness values irrespective of their thickness.

Film surface topography

A direct assessment of the surface topography of the films can be obtained by AFM. Figure 4 shows a series of images taken with this technique for surfaces of increasingly thick ZnO and SnO_2 thin films. RMS roughness values deduced from the analysis of these images are represented in Figure 5(a) in the form of a logarithmic diagram. This plot shows that the ZnO thin films are always rougher

than the SnO_2 ones. In addition, it clearly shows that while the roughness evolution can be described by a single linear correlation for the ZnO thin films, SnO_2 films present two different tendencies with an apparent inflexion point at around 100 nm, i.e., the thickness at which the microstructure of these films change from homogeneous to columnar (see Figure 1). The RMS values of the SnO_2 thin films with d<100 nm was very small, of the order of 0.1-0.2 nm, but sharply increased with thickness. For d>100 nm, the slope of the extrapolated straight line used to describe the roughness evolution have the values of 0.88 and 0.44 for ZnO and SnO_2, respectively. Within the premises of the DST, these slopes are equivalent to the growth exponent (β) and provide information about the mechanism of formation and growth of the films.[14,15]

Another important parameter used to describe the thin film growth mechanisms is the so called roughness exponent (α) which can be determined in different ways from the AFM images of the films surface. In our case, we have deduced the α values from the height to height correlation functions. A plot of this function estimated for the thin films with a thickness higher than 100 nm is represented in Figure 5(b). No calculations have been carried out with thinner films because the higher uncertainties associated with these less rough films. The plot shows that all the curves are characterized by a similar shape and a similar α value of 0.77, as deduced from the slope of the curves.

The roughness exponent α ($0 \leq \alpha \leq 1$) characterizes the short-range roughness of a self-affine surface, with larger values of α representing a locally smoother surface profile.[23] Reported α values for surface diffusion dominated film growth

are ~ 1.[24,25] The expected value of the growth exponent β in the case of normal scaling is 0.5 or less, with β ~ 0.25 for surface diffusion dominated film growth,[24] and β ~ 0.5 for the random deposition limit (without any surface relaxation process).[15] However, β values above 0.5 have been reported by some authors.[26-29] Recent studies suggest that this must be due to some nonlocal effects in surface dynamics,[30] e.g., step-edge barrier, shadowing effect, diffusional instability, etc. A shadowing effect takes place when particles arrive with tilted trajectories to a rough substrate, causing a preferential growth of the taller surface features that block the deposition on surface positions under their shadow. This is a non-local process known to lead to unstable growth with large β values (as high as β = 1) in surface evolution of various films.[26-28,31]

In our case, both SnO_2 and ZnO films have similar high values of the roughness exponent α (~0.77), which indicates that surface diffusion plays an important role on the surface morphology of both films, making the surfaces locally smooth. However, the measured β values (β = 0.88 for the ZnO film and β = 0.44 for the SnO_2 film) indicate that there must be some other mechanisms affecting the thin film growth besides surface diffusion. As it is in most magnetron sputtering depositions, shadowing effects are likely to be present in our films since the collision of the sputtered particles with the plasma gas causes a scattering of their trajectories. The effect of these collisions can be estimated by the thermalization degree (Ξ) [see ref. 32 and references within], defined as the ratio between the cathode-film distance and the thermalization length λ_T, where λ_T is the average distance that an atom has to travel in order to suffer enough collisions with other gas atoms to become thermalized. For our

deposition conditions we can estimate Ξ(Zn) ~ 0.22 and Ξ(Sn) ~ 0.15. These Ξ values imply that Zn atoms arrive more obliquely at the film surface than Sn atoms and that shadowing will be more important in ZnO growth, in agreement with the higher β value of these films. Other factors affecting the roughness of the films might also cause the observed differences in the growth exponent. Several experimental studies suggest that oriented grain growth can enhance the surface roughening during film growth[33,34] which, in turn, could further enhance the shadowing effects and lead to higher β values. This difference in growth behaviour might explain the different growth exponent values found in SnO_2 and ZnO films, in agreement with the fact that XRD measurements performed on our films show that ZnO films present a preferential (002) orientation.

Optical properties of thin films

The determined optical parameter functions of the SnO_2 and ZnO thin films measured by spectroscopic ellipsometry are reported in Figure 6. These parameter functions have been obtained after modeling the ellipsometric raw data as explained in the experimental section. As a justification of the model employed for the simulations, it is important to stress that both the specular X-ray reflectivity and AFM techniques have shown that the films are characterized by a nanoscopic roughness, where both the mean height and correlation length of the irregularities are much smaller than the wavelength of light in the visible and infrared part of the spectrum. For these rather flat surfaces it is expected that multiple scattering depolarizations are not important and therefore the

contribution of the field induced polarization of the surface to the far-field radiation pattern can be approximated by layers of a polarizable Bruggeman EMA model sandwiched between a perfect substrate and air, both taken as continuous media.[35] Then the Cauchy model was employed to determine the film thickness, roughness and real refractive index in the region where the films were transparent (500<λ<1400 nm).

According to the plots in Figure 6, the real part of the refraction index presents a smooth dispersion behavior for λ>450 nm. In the spectral region 300<λ<450 nm, this real part displays a variable dispersion due to the presence of the semiconductor band gap represented in our case by a Lorentz oscillator. From these results, it is important to stress that the real refraction index increases with the film thickness as noted in figures 6(a) and 6(c). Moreover, the extinction coefficient shows some absorption features for λ<450 nm, but becomes negligible in the region 450>λ>1400 nm (c.f., figures 6(b) and 6(d)), in agreement with the high transparency expected for these films. After fitting the experimental spectra, the obtained thickness values were close to nominal values, i.e., 21.9nm, 49.3nm, 94.9nm, 193.6nm, 343.4nm and 655.6nm for the ZnO samples and 24.5nm, 59.1nm, 109.3nm, 227.4nm, 427.4nm and 838.3nm for the SnO_2 films. These values are in relatively good agreement with those obtained by specular X-ray reflectivities for d≤100 nm and SEM analysis (see Figure 1). A similar agreement is found with the roughness results provided by AFM: the calculated roughness parameters of the films were 7.5nm, 27.5nm and 19.9nm for ZnO, and 2.9nm, 1.8nm and 5.3nm for SnO_2, for the films of nominal thicknesses of 200nm, 400nm and 800nm, respectively.

Spreading of silver on SnO_2 and ZnO thin film surfaces

A way of assessing the spreading of metals deposited onto real surfaces presenting a specific roughness is by following the deposition process by XPS and studying the evolution of the background of the spectra with the deposited amount. We have previously applied this methodology for a large variety of systems where the growth mechanism consisted on the formation of islands.[18,19,36,37] Herein, we have applied a similar methodology to ascertain the nucleation and growth behavior of silver on the surface of both SnO_2 and ZnO thin films. The idea of this methodology is to analyze the evolution of the backgrounds behind the elastic photoelectron peaks as a function of the amount of deposited material. As an example of the observed changes, Figure 7 shows four Ag3d photoemission peaks recorded for increased amounts of Ag deposited on a ZnO film with a thickness of 20 nm. For the sake of comparison, the spectra have been normalized to the height of the Ag3d5/2 elastic peak. Similar results were obtained on a ZnO thin film with a thickness of 200 nm and therefore higher roughness. This equivalence in spectral results for the two thin film thicknesses was also found when comparing the series of experiments performed on SnO_2 thin films (spectra not shown).

It is apparent in this figure, that the heights of the backgrounds behind the elastic peaks increase with the amount of deposited silver. The analysis of the shape of these backgrounds provides information about the growing mechanism of silver. Such an analysis has been carried out here for a series of experiments where the metal has been evaporated simultaneously on the surfaces of ZnO and SnO_2 films. This ensures that the two substrates receive the same amount of silver. Consequently, any difference in the growing mode of

silver on each particular substrate will be unequivocally evidenced by differences in both the intensity of the elastic Ag3d photoemission peaks and the height and shape of their inelastic backgrounds.

The spectra have been simulated with the QUASES software.[21] This analysis has shown that silver condenses on the surface of these two oxides in the form of three dimensional clusters, whose size and height increase with the amount of deposited metal. The average height of these islands (I_h) and the surface coverage (S_c) of the surface of the oxides determined with the QUASES calculations are represented in Figure 8 for the whole series of experiments carried out here on oxide thin films with a thickness of 20 nm. Equivalent curves were obtained by analyzing the results of the deposition experiments carried out on the SnO_2 and ZnO thin films with 200 nm thickness. For a better guidance, in this plot we have also included a series of the dotted lines representing theoretical curves obtained by assuming that the silver islands have a cubic form and that the product $I_h x S_c$ is constant and equivalent to the amount of deposited silver as indicated in the right axis of the plot.

Figure 8 reveals that for equivalent amounts of deposited silver, the coverage degree of the oxide surface is always greater (or alternatively, the islands´ heights smaller) on ZnO than on SnO_2. This behavior implies that under our experimental conditions silver wets and spreads better on the former oxide than on the latter. This is further sustained for the results corresponding to very low amounts of deposited silver on ZnO, clearly indicating that this metal completely spreads on the surface of this oxide and that it only starts to nucleate on its surface after the fourth evaporation experiment. Besides these trends, another interesting feature of the reported experiment are that total coverage implying

the complete coalescence of the silver islands only occurs after depositing an equivalent amount of silver of aproximately14 nm. It must be stressed that the similar results obtained when analyzing the deposition of silver on SnO_2 and ZnO of 200 nm thickness sustain that silver spreading mainly depends on the chemical nature of the sputtered deposited surfaces and that their roughness is a negligible factor for the control of silver wetting on these two oxide thin films.

Optical behavior of MOx/Ag/barrier/MOx structures

It is likely that the different spreading behaviour of silver on the two oxides may have an influence on the optical behaviour of the final stacked MOx/Ag/barrier/MOx structures. To test the final optical and low-emissivity properties of low-emissivity coatings, we have prepared structures of the type SnO_2/Ag/barrier/SnO_2, and ZnO/Ag/barrier/ZnO where both the oxide and the silver layers were deposited by MS according to experimental protocols resembling those utilized in the industry. Thickness of the oxides was kept around 40 nm, while the thickness of the Ag layer was 9 nm in the two cases to get identical contribution of Ag layer in both structures. Thicknesses of both dielectric layers were determined to get coatings with a green-bluish neutral color aspect both in transmission and in reflection modes. Optical properties of both structures are shown in Figure 9. These plots represent the transmission and the reflectivity of the two examined structures.

Thicknesses of the two dielectric layers were determined to get coatings with a green-bluish neutral color aspect both in transmission and in reflection modes.

Figure 9 shows the transmission and the reflectivity curves obtained for the two examined structures.

Besides, the emissivity at 100ºC of both structures yielded values of 0.09 for the SnO_2-based structure and 0.07 for ZnO-based structure, results that agree with the commonly accepted trend of lower emissivity values for ZnO-based structures. A similar conclusion can be gained by observing the plots in Figure 9 where small, though not negligible differences can be noticed between the SnO_2 and ZnO structures, with a slightly higher transmission in the IR range for the former.

The different behavior found for the two structures can be accounted for by assuming a different distribution of silver on the two oxides and/or that the oxide themselves present different roughness. Referring to this latter point, the morphological analysis of the oxide thin films reported previously has clearly evidenced that for all range of investigated thicknesses ZnO prepared by MS is rougher than SnO_2. Hence, if this were the sole factor contributing to the different emissivity of the two structures, SnO_2-based structures should have a superior performance than the ZnO ones. Therefore, we have to admit that the more favorable tendency of silver to spread onto the surface of ZnO surface than on that of SnO_2 evidenced by our silver evaporation experiment should be the main factor contributing to the superior performance of the ZnO based stacked structure. As it is shown in Figure 8, for a thickness of 9 nm in our experiment (note that the experimental conditions are different than those used to prepare the silver film in the stacked structures which implies the use of magnetron sputtering), the coverage degree of the substrate is higher than 80% on ZnO, while it is only around 60% for SnO_2, Assuming a similar behavior for

MS layers, a higher coverage degree (and therefore a higher percolation and continuity of the metal sheet) in the stacked structure should reduce the sheet resistivity of the silver deposited onto ZnO and thus generate a lower emissivity value for the whole coating.

4. Summary and Conclusions

In this work we have primarily studied the evolution of roughness of ZnO and SnO_2 sputtered layers prepared by simulating industrial conditions of deposition. Then, we have analyzed the wetting and coverage degree of Ag deposited on these thin films in order to clarify the different emissivity behavior of MeOx/Ag/barrier/MeOx low-emissivity coatings. The analysis of the roughness evolution of the films by using the principles of the DST shows that the higher roughness presented by the ZnO thin films must be mainly attributed to an enhancement of the shadowing effects due to the preferential growth of these crystalline films according to a given crystallographic plane. Despite the higher roughness of the ZnO thin films, silver appears to spread more efficiently on the surface of this material than on that of SnO_2 thin films. Coverage degree by the silver layer, instead of roughness of the oxide layers, has been revealed as the main factor explaining the lower emissivity values of ZnO/Ag/barrier/ZnO structures. Future works to improve emissivity of this type of structures should therefore concentrate in getting higher coverage degrees of the oxide (i.e., improve the wetting by the deposited metal), rather than on reducing the roughness of the oxide layers.

Acknowledgements

We thank the Junta de Andalucía (Projects P09-CTS- 5189, TEP5283 and FQM-6900) and the Ministry of Economy and Competitiveness (Projects CONSOLIDER CSD2008-00023, MAT2010-21228, and MAT2010-18447) for financial support. JC González thanks the Spanish Scientific Research Council (CSIC) for a JAE-Doc contract (2009-2012) at the ICMSE-CSIC-US.

References

[1] C.G. Granqvist, Adv. Mater. **15**, 1789 (2003)

[2] C. Guillén, J. Herrero, Thin Sol. Films **520** 1 (2011)

[3] J. Kulczyk-Malecka, P.J. Kelly , G. West, G.C.B. Clarke, J.A. Ridealgh, Thin Sol. Films **520**, 1368 (2011)

[4] B. P.Jelle, A. Hynd, A. Gustavsen, D. Arasteh, H. Goudey, R. Hart, Solar Ener. Mater. Solar Cells **96**, 1 (2012)

[5] P. Grosse, R. Hertling, T. Miiggenburg, J. Non-Crystal. Solids **218** 38 (1997)

[6] E. Ando, M. Miyazaki, Thin Sol. Films **516**, 4574 (2008)

[7] M. Rubin, D. Arasteh and J. Hartmann, Int. Comm. Heat Mass Transfer **14**, 561 (1987)

[8] J. Mohelnikova, Const. Build. Mater. **23**, 1993 (2009)

[9] G.T. West, P.J. Kelly, J.W. Bradley, IEEE Transact. Plasma Sci. **38**, 3057 (2010)

[10] K. Kato, H. Omoto, T.Tomioka, A. Takamatsu, Solar Ener. Mater. Solar Cells, **95**,2352 (2011)

[11] Z.B. Huang, W.C. Zhou, X.F. Tang, D.M. Zhu, F. Luo, Thin Sol. Films **519**, 3100 (2010)

[12] J. Szczyrbowski, G. Brauer, M. Ruske, H. Schilling, A. Zmelty, Thin Sol. Films **351**, 254 (1999)

[13] R.J. Martin-Palma, L. Vazquez, J.M. Martinez-Duart, Malats-Riera, Solar Ener. Mater. Solar Cells **53**, 55 (1998)

[14] A.-L. Barabasi, H.E. Stanley, *Fractal Concepts in Surface Growth*, CambridgeUniversity Press, Cambridge, England, 1994.

[15] M. Pelliccione, T.-M. Lu, *Evolution of Thin Film Morphology: Modeling and Simulations*, Springer Series in Materials Science Vol. 108, Springer, New York, 2008

[16] S.Tougaard, J.Vac.Sci. & Technol.A, **14**, 1415, (1996)

[17] S. Tougaard, Surf. Interf. Anal. **26**, 249 (1998).

[18] A.I. Martín-Concepción, F. Yubero, J.P. Espinós, A.R. González-Elipe, S. Tougaard, J. Vac. Sci. & Technol. A **21** 1393 (2003)

[19] F.Gracia, F.Yubero, J.P.Espinós and A.R.González-Elipe, Appl. Surf. Sci. **252**, 189 (2005)

[20] H. J. Glässer. *Large Area Glass Coatings*. Von Ardenne Anlagentechnik GMBH 2000, p. 188

[21] S.Tougaard, *QUASES, Software package for quantitative XPS/AES of surface nanostructures by inelastic peak shape analysis*, www.QUASES.com

[22] S.Tanuma, C.J.Powell, D.R.Penn, Surf.Interf. Anal., **21**, 165 (1993).

[23] J. Krim, J.O. Indekeu, Phys. Rev. E **48**, 1576 (1993)

[24] S. Das Sarma, P. Tamborenea, Phys. Rev. Lett. **66**, 325 (1991)

[25] Z.J. Liu, N. Jiang, Y.G. Shen, Y.W. Mai, J. Appl. Phys. **92**, 3559 (2002)

[26] M.A. Auger, L. Vazquez, R. Cuerno, M. Castro, M. Jergel, O. Sanchez, Phys. Rev. B **73**, 045436 (2006)

[27] A. Yanguas-Gil, J. Cotrino, A. Barranco, A.R. Gonzalez-Elipe, Phys. Rev. Lett. **96**, 236101 (2006)

[28] S. Yim, T.S. Jones, Phys. Rev. B **73**, 161305 (2006)

[29] J.G. Yu, J.G. Amar, Phys. Rev. E **66**, 021603 (2002)

[30] W. Schwarzacher, J. Phys. Condens. Matter 16, 859 (2004)

[31] M. Pelliccione, T. Karabacak, T.-M. Lu, Phys. Rev. Lett. 96, 146105 (2006)

[32] J.M. Garcia-Matin, R. Alvarez, P. Romero-Gomez, A. Cebollada, A. Palmero, Appl. Phys. Lett. **97**, 173103 (2010)

[33] J.H. Xu, L.H. Yu, I. Kojima, J. Appl. Phys. **94**, 6827 (2003)

[34] X. Jiang, B. Hao, Journal of Crystal Growth **312**, 1844 (2010)

[35] D.E. Aspnes, J. B. Theeten and F. Hottier. Phys. Rev. B. **20**, 3292 (1979)

[36] C.Mansilla, F. Gracia, A.I. Martin-Concepción, J.P. Espinós, J.P. Holgado, F. Yubero, A.R. González-Elipe, Surf. Interf. Anal., **39**, 331 (2007).

[37] J.P.Espinós, A.I.Martín-Concepción, C.Mansilla, F.Yubero, A.R.González-Elipe, J. Vac. Sci. Technol. A **24**, 919 (2006)

Figure captions

Figure 1.- Cross section SEM images of the SnO_2 (left) and ZnO (right) thin films. The white arrow in the former signals the limit of the film where the nanocolumnar growth starts

Figure 2.- Glancing angle (lower part of the plots) and Bragg-Brentano (upper part of the plots) XR diagrams of SnO_2(left) and ZnO (right) thin films of different thickness. The diagrams have been vertically displaced for convenience.

Figure 3.- Experimental and calculated X-ray reflectivity curves of ZnO (top) and SnO_2 (bottom) thin films of 20 (left) and 100 (right) nm.

Figure 4.- AFM images of the surface of ZnO and SnO_2 thin films of increasing thickness. ZnO: a)20 nm; b)100 nm; c)200 nm; d) 400 nm; e) 800 nm. SnO2: f)20 nm; g)100 nm; h) 200 nm; i) 400 nm; j) 800 nm.

Figure 5.- (a) Representation of the roughness versus the thin film thickness for ZnO and SnO2 thin films showing the fitting lines to calculate the growth exponent (β). (b) Representation in a normalized scale of the height to height correlation function and calculation of the roughness exponent (α), where the graphs have been overlapped for better comparison.

Figure 6.- Refraction index (top) and extinction coefficient (bottom) curves of SnO_2 (left) and ZnO(right) thin films of different thickness. The arrows indicate how the thickness of the films increases.

Figure 7. Ag3d spectra for Ag deposited by thermal evaporation on the surface of a ZnO film, for the indicated amounts of nominal thickness of silver. The

spectra have been intensity normalized to the height of the elastic Ag3d5/2 peak.

Figure 8.-Representation of the island height against the surface coverage for successive evaporations of silver on the surface of ZnO and SnO_2 thin films. The dotted lines represent theoretical curves corresponding to equivalent amounts of silver calculated by assuming that $I_h x S_c$=cte. Estimated error bars are indicated.

Figure 9 Dependence with wavelength of a) reflection and b) transmission coefficients of SnO_2/Ag/barrier/SnO_2 and ZnO/Ag/barrier/ZnO coatings. The reflection coefficients in a) were obtained for both the glass substrate side (Glass) and the thin film side (Layer)

Figure 1

Click here to download high resolution image

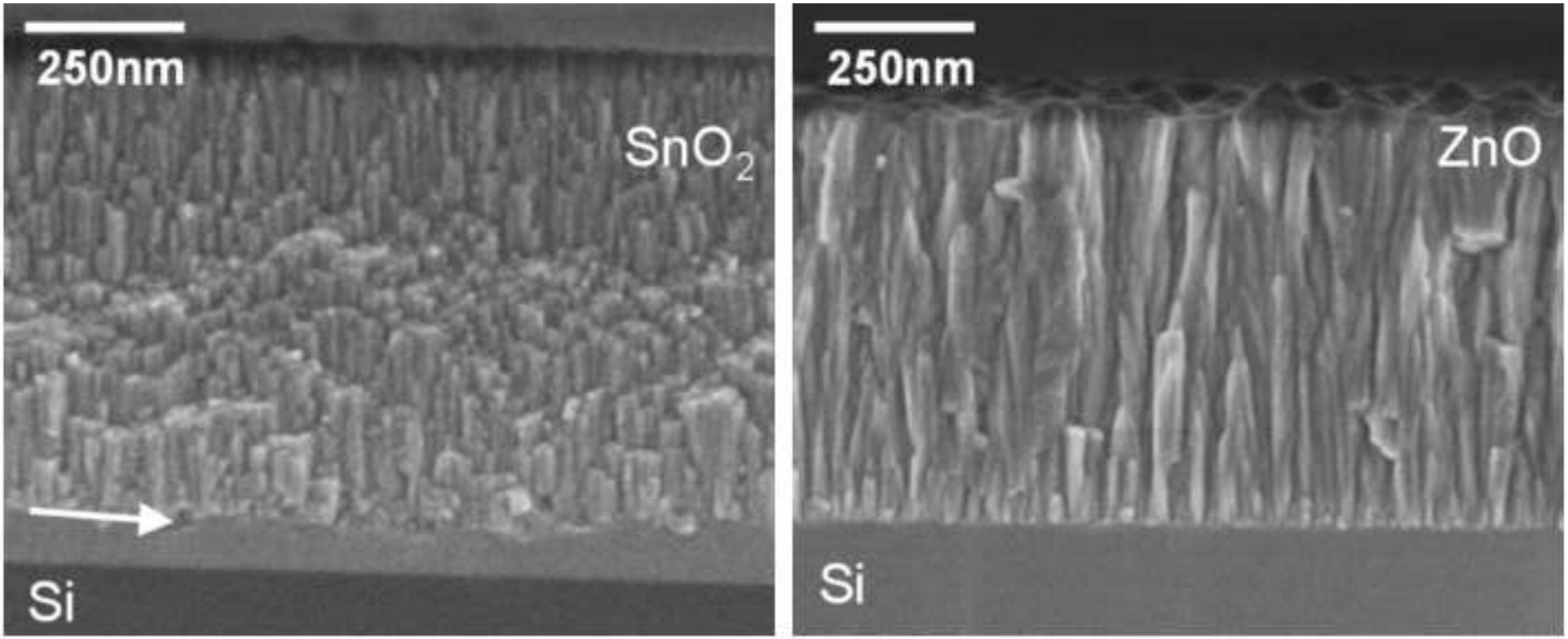

Figure 2

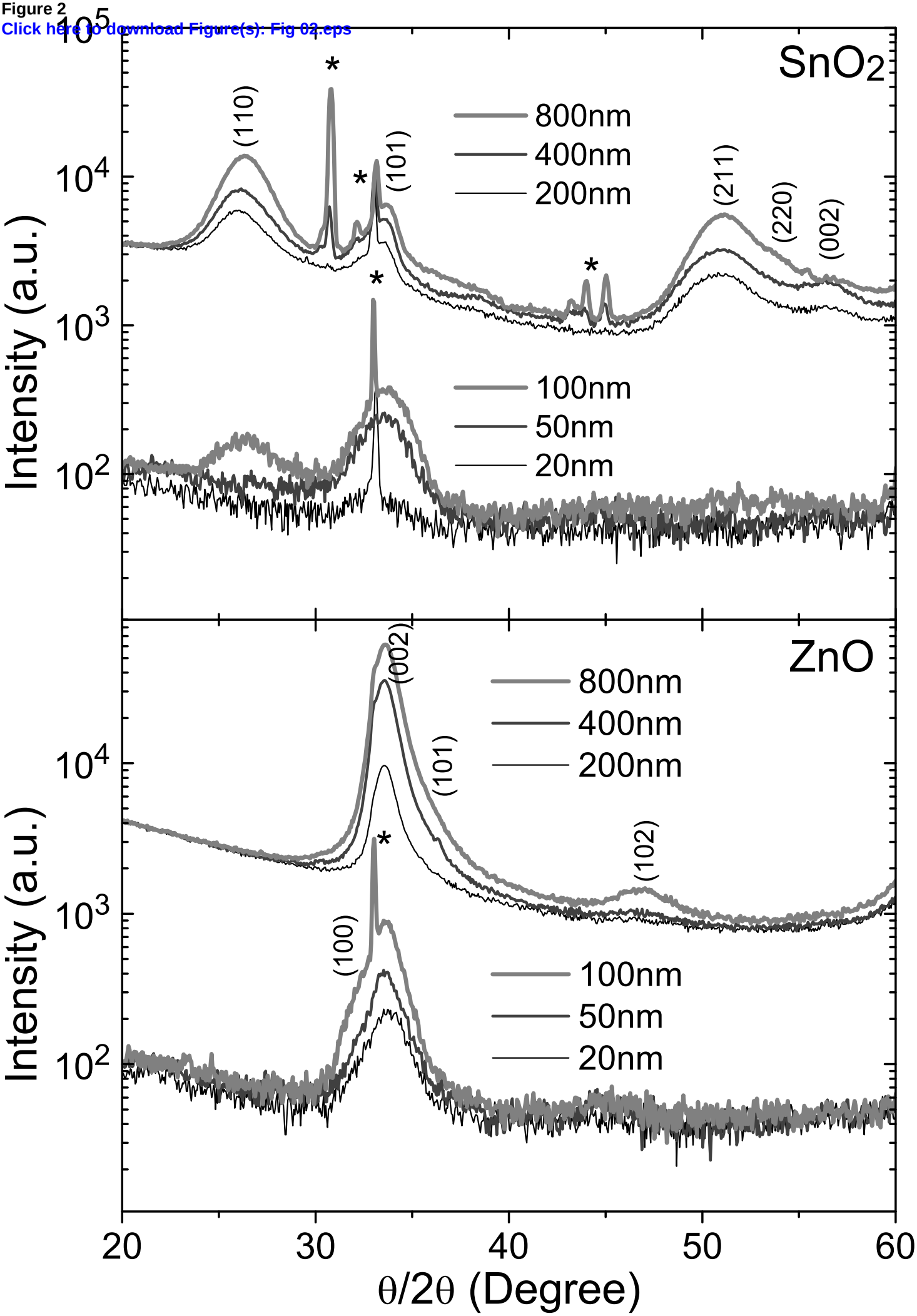

Figure 3
Click here to download Figure(s): Fig 03.eps

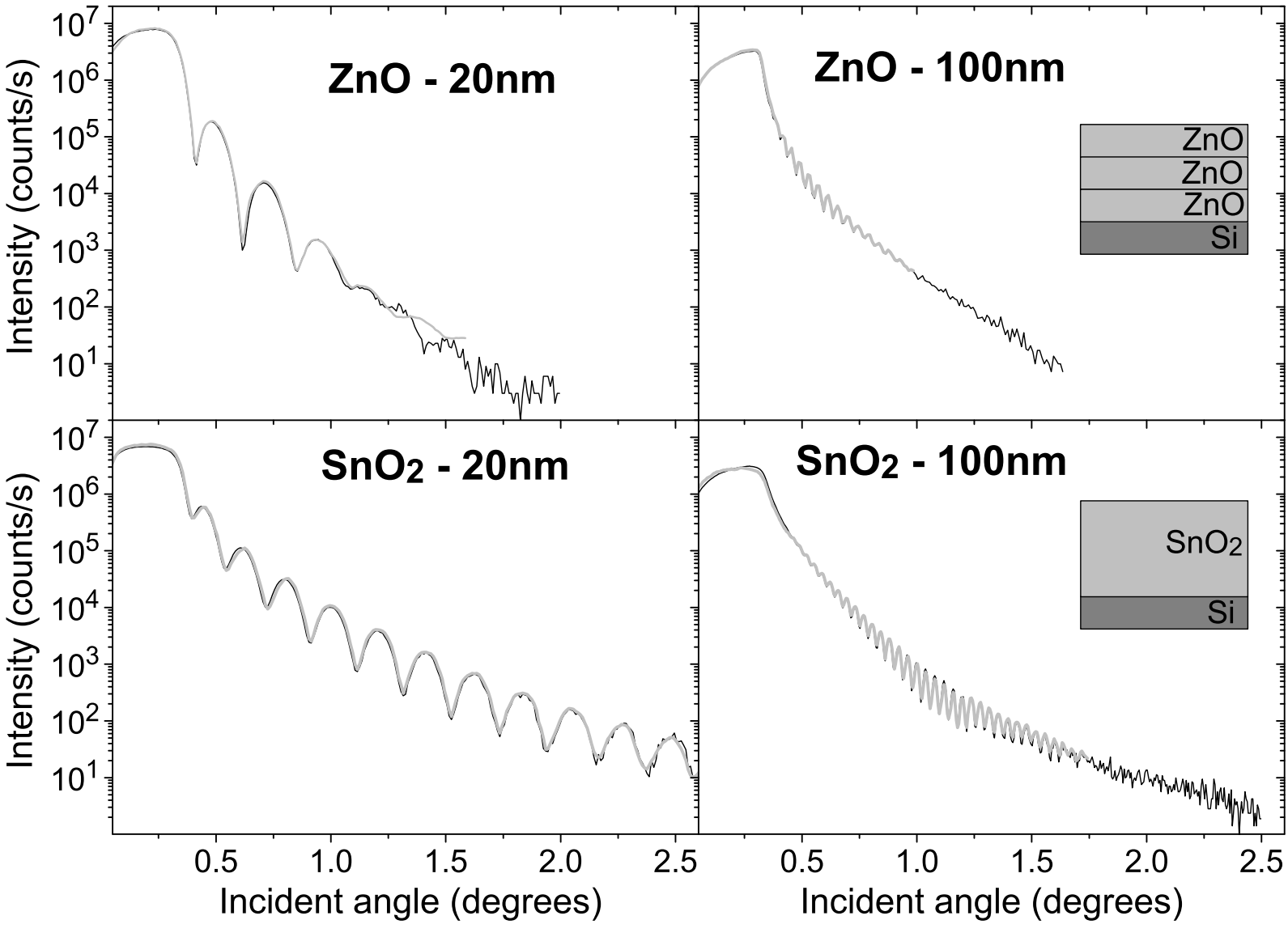

Figure 4

Click here to download high resolution image

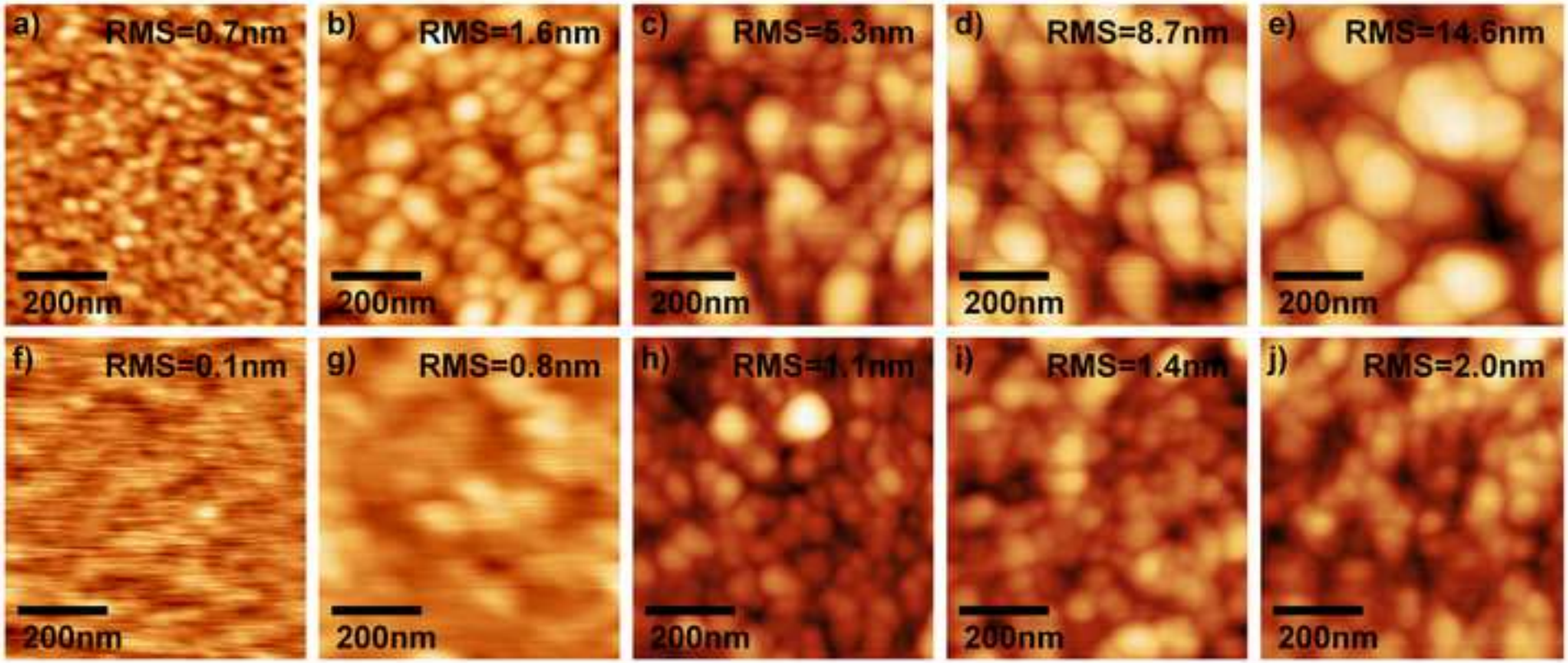

Figure 5

Click here to download Figure(s): Fig 05.eps

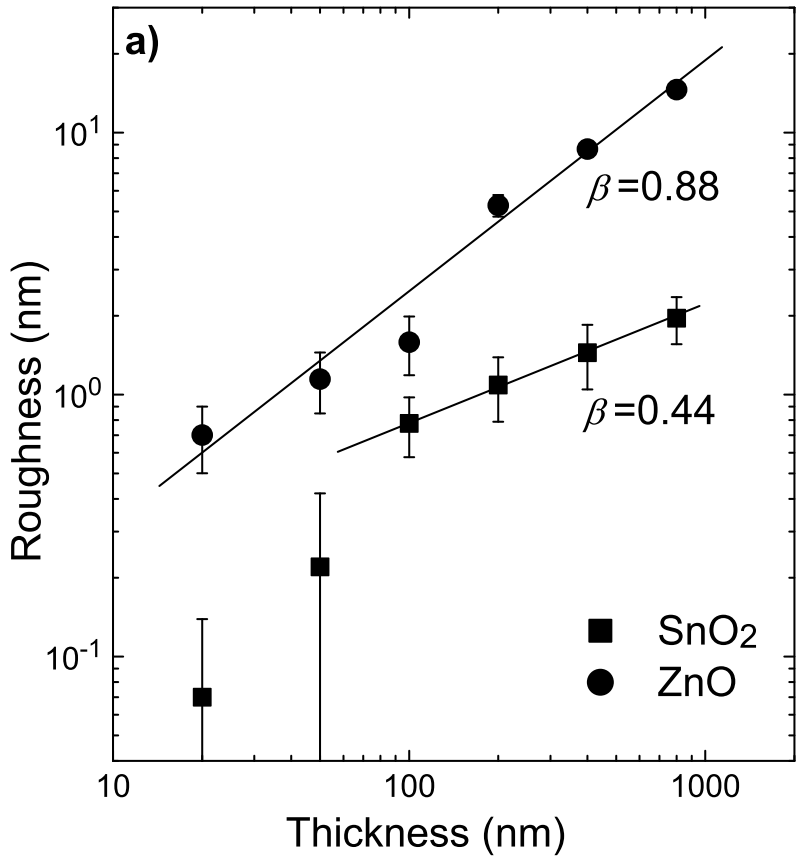

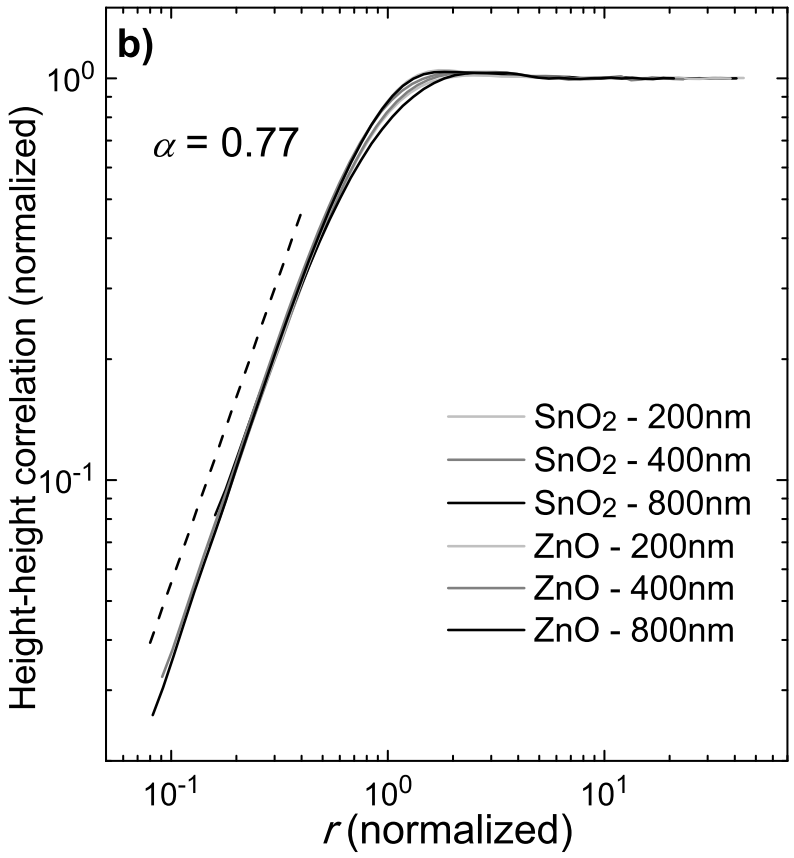

Figure 6
Click here to download Figure(s): Fig 06.eps

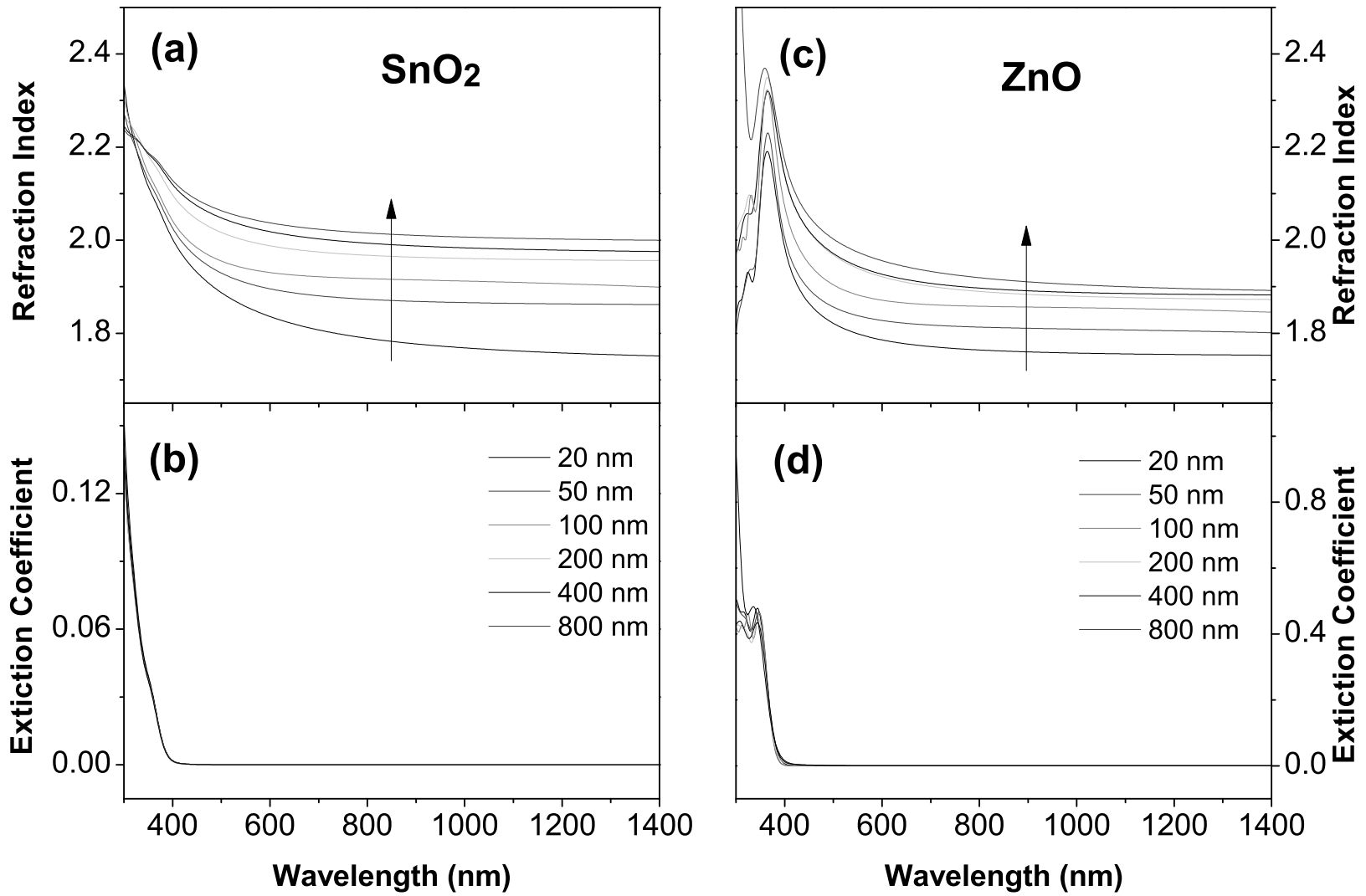

Figure 7
Click here to download Figure(s): Fig 07.eps

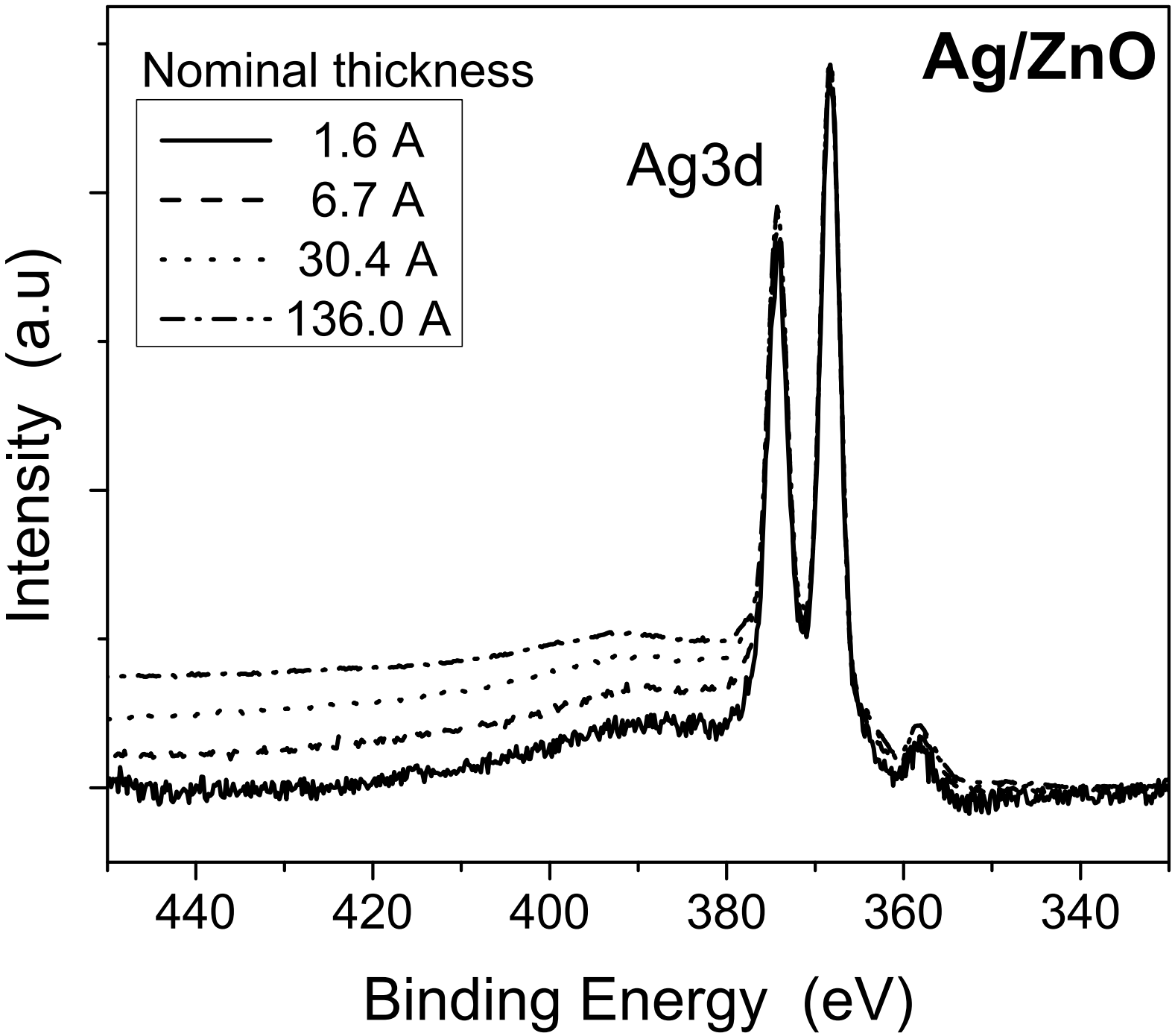

Figure 8
Click here to download Figure(s): Fig 08.eps

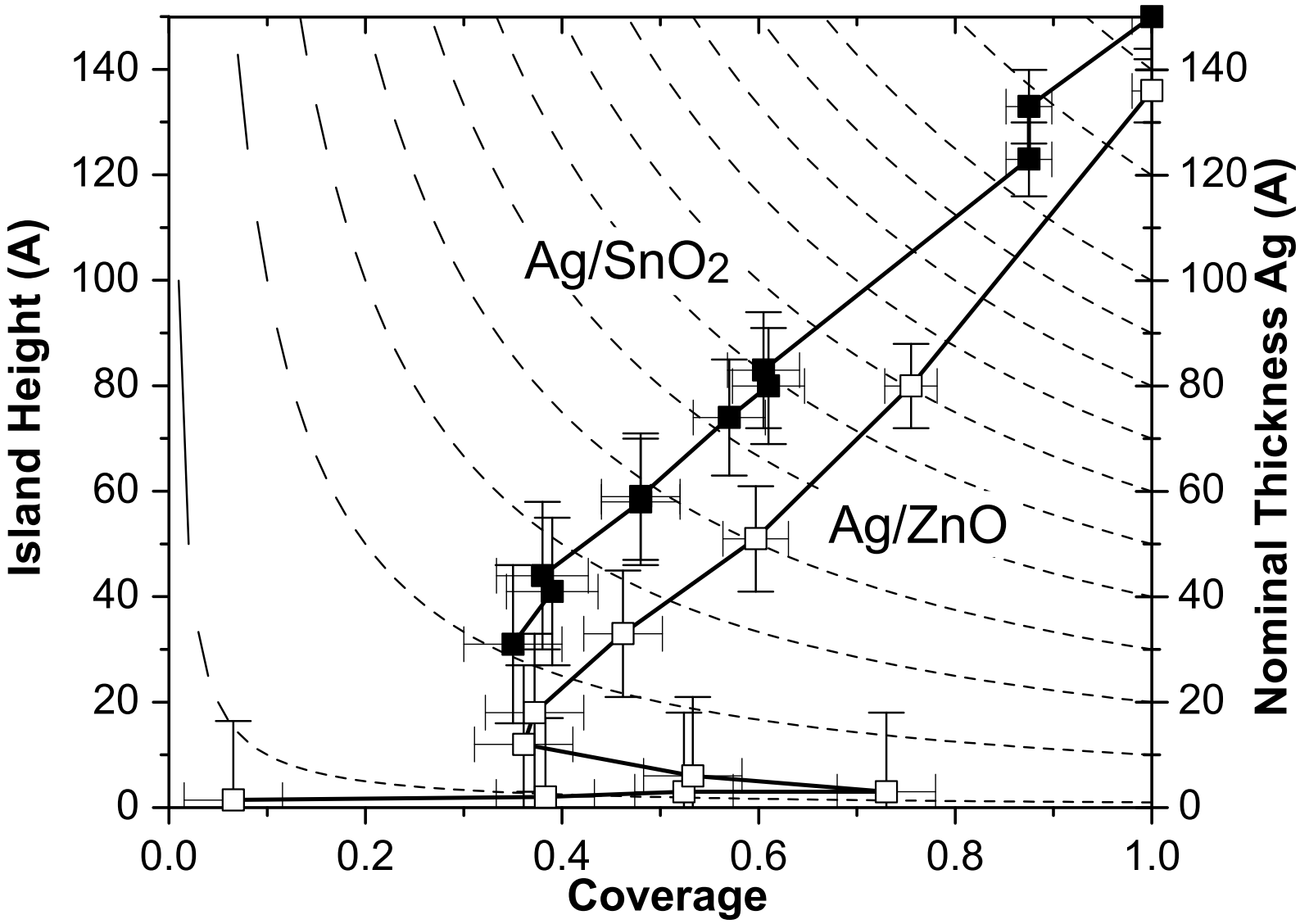

Figure 9
Click here to download Figure(s): Fig 09.eps

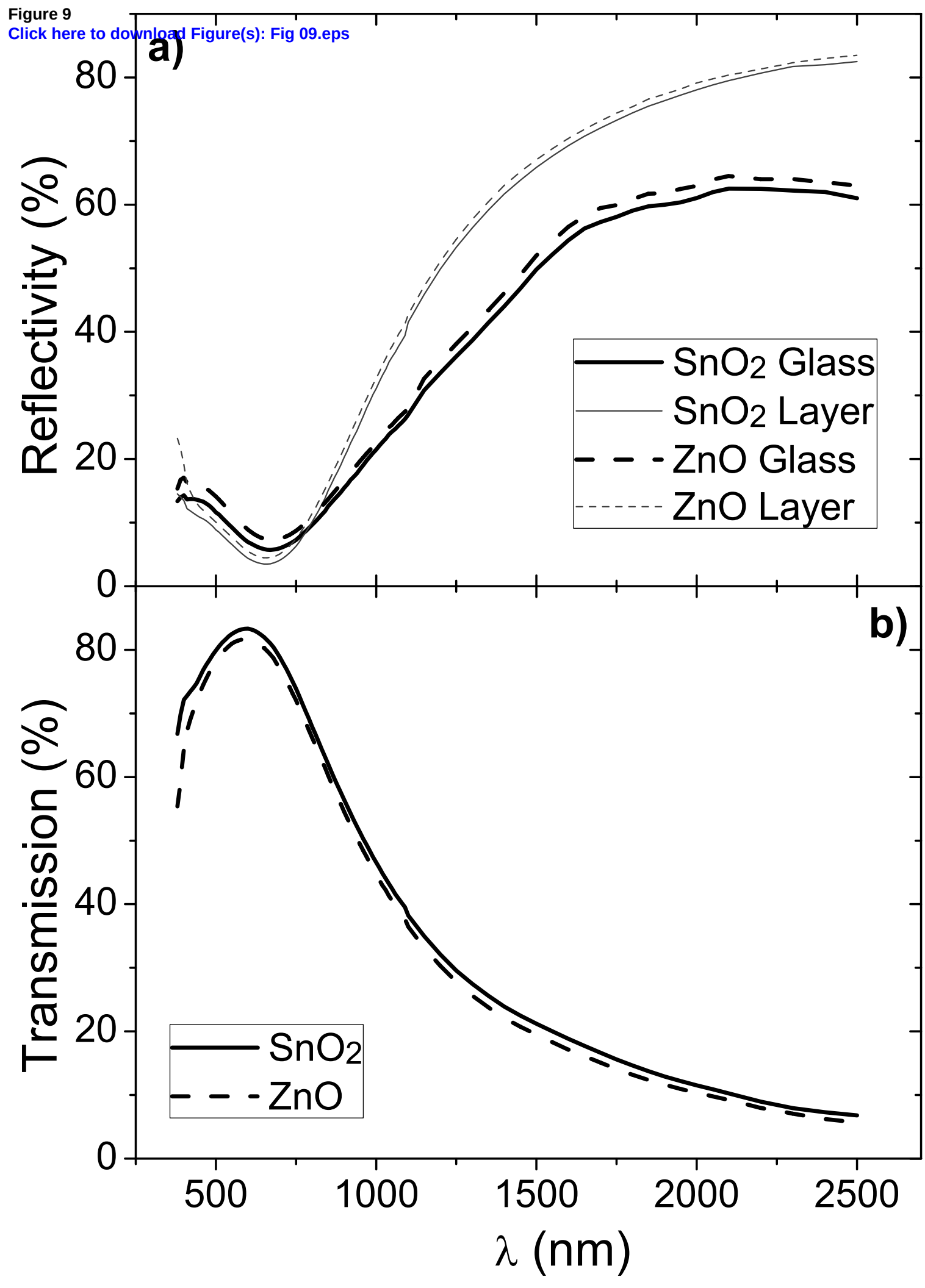

Table(s)

Table 1.- Experimental conditions of sputtering deposition

Material	Target	Total pressure (mbar)	O_2 pressure (mbar)	Power (W)	Power density W/cm^{-2}
SnO_2	Tin	1×10^{-3}	5×10^{-4}	150	3.3
ZnO	Zinc	1×10^{-3}	8×10^{-4}	300	6.5

Table 2.- Structural and microstructural parameters of the films deduced from their XRD and X-ray reflectivity analysis

Sample	Size of crystalline domains (nm)	Average Density (g/cm^3)	Surface Roughness (nm)	Substrate-interface Roughness (nm)
SnO_2				
20 nm	3.4	5.95	0.5	0.5
50 nm	3.3	6.60	0.9	0.6
100 nm	3.1	6.83	1.1	0.4
200 nm	7.3			
400 nm	6.6			
800 nm	6.5			
ZnO				
20 nm	4.0	4.64	1.0	1.1
50 nm	4.7	4.97	1.0	1.0
100 nm	4.6	4.84	1.0	1.0
200 nm	8.2			
400 nm	6.6			
800 nm	6.4			